Lab on a Chip

Accepted Manuscript

ROYAL SOCIETY OF CHEMISTRY

www.rsc.org/loc

Lab on a Chip

RSCPublishing

Using Patterned Grating Structure to Create Lipid Bilayer Platforms Insensitive to Air Bubbles

Cite this: DOI: 10.1039/x0xx00000x

Chung-Ta Han, and Ling Chao*

Received ooth January 2012,
Accepted ooth January 2012

DOI: 10.1039/x0xx00000x

www.rsc.org/

Supported lipid bilayers (SLBs) have been used for various biosensing applications. The bilayer structure enables embedded lipid membrane species to maintain their native orientation, and the two-dimensional fluidity is crucial for numerous biomolecular interactions to occur. The platform integrated with a microfluidic device for reagent transport and exchange has great potential to be applied with surface analytical tools. However, SLBs can easily be destroyed by air bubbles during the assay reagent transport and exchange. Here, we created patterned obstacle grating structured surface in a microfluidic channel to protect SLBs from being destroyed by air bubbles. Unlike all of the previous approaches using chemical modification or adding protection layers to strengthen lipid bilayers, the uniqueness of this approach is to use the patterned obstacles to physically trap water above the bilayers to prevent the air–water interface from directly contacting and peeling the bilayers. We showed that our platform with certain grating geometry criteria can provide promising protection to SLBs from air bubbles. The required obstacle distance was found to decrease when we increased the air-bubble movement speed. In addition, the interaction assay result from the streptavidin and biotinylated lipid in the confined SLBs suggested that receptors at the SLBs retained the interaction ability after air-bubble treatment. The results showed that the developed SLB platform can preserve both high membrane fluidity and high accessibility to the outside environment, which have never been simultaneously achieved before. Incorporating the built platforms with some surface analytical tools could open the bottleneck of building highly robust in vitro cell-membrane-related bioassays.

INTRODUCTION

Supported lipid bilayers (SLBs) have been used in various biosensing applications.[1-3] The bilayer structure enables embedded membrane species to maintain their native orientation and conformation, and the two-dimensional fluidity is crucial for numerous biomolecular interactions to occur.[4, 5] Incorporating SLBs into cell membrane-related bioassays, such as drug screening[6, 7] and toxin detection[8, 9], have been considered crucial for obtaining accurate assay results and for discovering new phenomena. However, conventional SLBs easily delaminate after being exposed to air–water interfaces. In the steps of various bioassays, the samples are inevitably exposed to air during sample transport or reagent exchange, causing difficulty in obtaining robust assay results.[10, 11] For example, when surface plasmon resonance and quartz crystal microbalance techniques are used for detecting biomolecular interactions, multiple reagent additions and washes are required to obtain binding and equilibrium constants. Developing SLB platforms that are insensitive to the air–water interface and retain their bilayer structure and fluidity is critical for broadening the capability of developing cell-membrane-related in vitro assays.

Several approaches have been developed for preventing SLBs from delaminating after being exposed to an air–water interface. Some of these studies have involved using polymerizable lipids to cross-link the lipid bilayer structure [12-14] or lipopolymers—lipids with polymers attached to the head groups—to increase the rigidity and degree of membrane hydration.[15] Other approaches have involved modifying solid support surfaces by using a tethered cholesteryl group,[16] zirconium phosphate,[17, 18] γ-aminopropyl saline,[19-21] or negatively charged polydimethylsiloxane (PDMS)[22] to provide strong interactions between the support surfaces and lipid bilayers to overcome the interfacial peeling force. These studies have successfully developed reinforced lipid bilayers that can retain their integrity against air–water interfacial force; however, modifying the chemical structure of the lipid or strongly tethering the lipid membrane to the modified supports can alter the native environment for certain membrane species. Another category of studies has involved adding biomolecules, such as proteins[9, 23] and disaccharides[24-29] to form protective layers above the membrane for enhancing the bending modulus of the membrane and preventing the lipid bilayer from curling during delamination. Although most of the studies in this category have developed air-stable lipid bilayers exhibiting promising stability and fluidity, the steric hindrance caused by the protective layer can block the accessibility of analytes in an aqueous solution to the target receptors located on the lipid bilayer. Overall, all of the previous approaches achieve air stability by increasing the membrane rigidity and thus could

influence some membrane properties crucial for the interested biological phenomena to occur.

In this study, we developed an SLB platform with patterned obstacle gratings that can prevent the lipid membrane from directly contacting the air–water interface when an air bubble is introduced during the reagent exchange. Unlike all of the previous studies using chemical methods to modify the surface to create air-stable SLBs, we used a physical method inspired from previous observations that trenches or pores on a hydrophilic surface can trap some water[30, 31]. We expected that if lipid bilayers can be confined in the trenched regions, they could be protected by the tapped water and not directly affected by the deleterious air–water interfacial force. The gratings were patterned perpendicular to the reagent flow direction in a microchannel to achieve optimal water-retention ability between the grating obstacles. To determine the appropriate geometry criterion for the grating structure to function, we prepared a range of grating distances and examined the membrane integrity and mobility by using fluorescence microscopy and fluorescence recovery after photobleaching (FRAP) before and after air-bubble treatment. In addition, we used a streptavidin-biotinylated lipid as a model system to demonstrate that not only the lipid bilayer integrity but also the receptor–ligand interaction can remain in the developed platform after air-bubble treatment.

EXPERIMENTAL SECTION

Materials 1,2-dioleoyl-sn-glycero-3-phosphocholine (DOPC) was purchased from Avanti Polar Lipids (Alabaster, AL, USA). Texas Red 1,2-dihexadecanoyl-sn-glycero-3-phosphoethanolamine, triethylammonium salt (Texas Red® DHPE), *N*-((6-(biotinoyl)amino) hexanoyl)-1,2-dihexadecanoyl-sn-glycero-3-phosphoethanolamine, triethylammonium salt (Biotin-X DHPE), and Alexa Fluor® 488-conjugated streptavidin were purchased from Life Technologies (Grand Island, NY, USA). Bovine serum albumin (BSA) was purchased from Sigma-Aldrich (St. Louis, MO, USA).

Preparing Substrates Exhibiting a Photoresist Grating Structure by Using Photolithography A glass coverslip substrate exhibiting a micron-sized photoresist grating structure was prepared using photolithography. The bare glass was cleaned by RCA cleaning procedure (5:1:1 H_2O:H_2O_2:NH_4OH) before the performing the microfabrication process. A thin film of negative photoresist SU-8 2002 (MicroChem Corp., USA) was spin-coated on the glass substrate at 3000 rpm for 30 s to achieve the desired thickness (approximately 2 μm) and soft-baked at 90 °C for 1 min. The substrate was then placed under a chrome mask with a desired grating pattern and exposed to ultraviolet radiation at exposure energy of 80 mJ/cm^2. The substrate was then postbaked at 95 °C for 2 min and developed in a SU-8 developer (MicroChem Corp., USA) through gentle shaking for 20 s. The glass substrate with the photoresist pattern was rinsed with isopropyl alcohol and dried using nitrogen gas. The substrate was then hard-baked at 150 °C for 1 h to enhance the attachment of SU-8 to the glass.

Preparation of Large Unilamellar Vesicles The purchased lipids were mixed in a chloroform solution for obtaining desired compositions. The chloroform solvent was then removed using nitrogen, leaving a lipid cake at the bottom of the container. The lipid cake was then placed in a vacuum for 5 h to ensure the complete removal of the residual chloroform. The lipids were then reconstituted in a HEPES buffer (10 mM HEPES and 123 mM NaCl, pH 7.4) at a concentration of 2 mg/mL, and extruded through a 50-nm polycarbonate filter 19 times by using an Avanti Mini-Extruder (Alabaster, AL, USA) to form large unilamellar vesicles (LUVs).

Formation of Supported Lipid Bilayers on the Substrate with a Photoresist Grating Structure inside a Microfluidic Device The prepared substrate with an SU-8 photoresist grating structure was cleaned using argon plasma for 10 min. The plasma can change the wetting properties and surface roughness of the SU-8.[32, 33] A PDMS slab with a microchannel (100 μm × 500 μm × 1.5 cm) was then treated with oxygen plasma for 30 s and sealed with the glass coverslip. The LUV solution was then flowed into the microchannel, followed by a 10-min incubation for vesicle deposition to form SLBs on the area of bare glass that was not covered with the SU-8 grating. The excess lipid vesicles were then washed away by using water.

Dehydration and Rehydration of the Supported Lipid Bilayer by Introducing an Air-Bubble into the Microchannel An air bubble was pumped into the microchannel at a flow rate of either 3 μL/min (60 mm/min) or 300 μL/min (6000 mm/min) to create an air–water interface passing through the SLB platform inside the microchannel. The size of the bubble was approximately 100 μL, and it required 33 min or 3.33 min to pump the entire bubble through the channel. The beginning of the dehydration state was defined as the time immediately after the air bubble entered the microchannel. The beginning of the rehydration state was defined as the point at which the air bubble left the microchannel completely.

Fluorescence Microscopy and Fluorescence Recovery after Photobleaching A 200-mW diode-pumped solid-state green laser module (Unice, Taiwan) at 532 nm was used for photobleaching Texas Red DHPE in a lipid bilayer sample for 0.1 s. The bleached spot can be fitted with a Gaussian profile with a half-maximum width of approximately 10 μm. The recovery time evolution images of a bleached spot was recorded using an inverted microscope (Olympus IX81, Olympus, Japan) equipped with a charge-coupled-device camera (ORCA-R2, Hamamatsu, Japan) and a 20× objective lens (UPLSAPO, Olympus, Japan). The intensity recovery data in the region of interest were fitted using MATLAB (MathWorks, Natick, MA, USA) to obtain the diffusion coefficient of the SLB. The details of the fitting algorithm are shown in our previous study[34].

Streptavidin-Biotinylated Lipid Interaction Test DOPC SLBs doped with 0.5 mol% of Biotin-X DHPE were

formed on a glass substrate with or without SU-8 grating obstacles in a microchannel. An air bubble was then pumped through the microchannel at a flow rate of 3 μL/min (60 mm/min). Subsequently, 250 μg/mL of BSA solution was flowed into the microchannel and incubated for 30 min to prevent the subsequent nonspecific binding of streptavidin to the region not covered with the SLBs. The excess BSA solution was then flushed away, and 10 μg/mL of Alexa Fluor® 488-conjugated streptavidin was flowed in and incubated for 30 min for the binding. The excess streptavidin in bulk was flushed away later. A control experiment was conducted without introducing an air bubble into the microchannel. The amount of streptavidin binding to the biotinylated lipid in the membrane was determined by observing the measured fluorescence intensity after the background subtraction.

RESULTS AND DISCUSSION

Patterned Photoresist Grating for Preventing the Air–Water Interface from Directly Contacting the Supported Lipid Bilayer To develop an air-stable SLB platform, we constructed obstacle gratings on a glass surface and deposited lipid membranes in the regions confined by the obstacles. We used a photoresist, SU-8, as our obstacle material so that we could easily use photolithography to fabricate a patterned obstacle grating structure at various sizes and geometries on glass surfaces. In addition, lipid vesicles can be deposited to form SLBs only on glass, not on SU-8 photoresist material. Therefore, we obtained pieces of SLB confined by the photoresist obstacles. As shown in Figure 1, when the air–water interface front moved, the SLB were preserved because the obstacle gratings trapped some water and prevented the air–water interface from directly contacting the SLB on the bottom surface. Although the trapped water layer above the SLB could later evaporate from the surface, no substantial interfacial force in the peel-off direction could be directly applied to the SLB, and the bilayer structure was preserved.

As shown in Figure 1(a), the obstacle grating was set perpendicular to the flow direction in a microchannel to maximize the size of each piece of the SLB confined in the obstacle grating. A large continuous piece of lipid bilayer is usually desirable in real applications because of the fewer possible disturbances from the grating obstacles. According to the proposed mechanism, the obstacles need to orientate in a way so that they can truncate the interfacial moving front before the water receding tail contacts the lipid bilayer. When the obstacle grating is set perpendicular to the flow direction, the traveling distance of the air-water interface between the two obstacles is the shortest, which maximizes the possible largest distance between the two obstacles that would not allow the interface to contact the SLB.

Figure 1(a)(b)(c) shows the top view fluorescence images when an air-bubble was arriving in the SLB platform, when the platform was under the air-bubble and when the air-bubble was leaving the platform. The bright curved rings across the channel in (a) and (c) are the front and back of the air-bubble. 0.5 mol% Texas Red DHPE was added to the lipid membrane to reveal the locations of the confined SLBs (bright) and the obstacle grating (dark). The fluorescence microscopy allows us to microscopically observe whether the SLBs were destroyed. Dark defects or scratches at the lipid membranes and bright debris in the solution should be observed if the SLBs delaminated. The similar uniform looks before and after an air-bubble suggests that the fluorescent SLB remained at the original place after air-bubble treatment. We also observed a slightly brighter region around the dark grating obstacles when the SLBs were below an air bubble. The brighter region was not observed when the SLBs were fully under water. Since SU-8 is shown to be hydrophilic after oxygen plasmon[32] as what we did in this work, water menisci curving upwards at the sides of the obstacles could form. The brighter region is probably from the meniscus light diffraction.

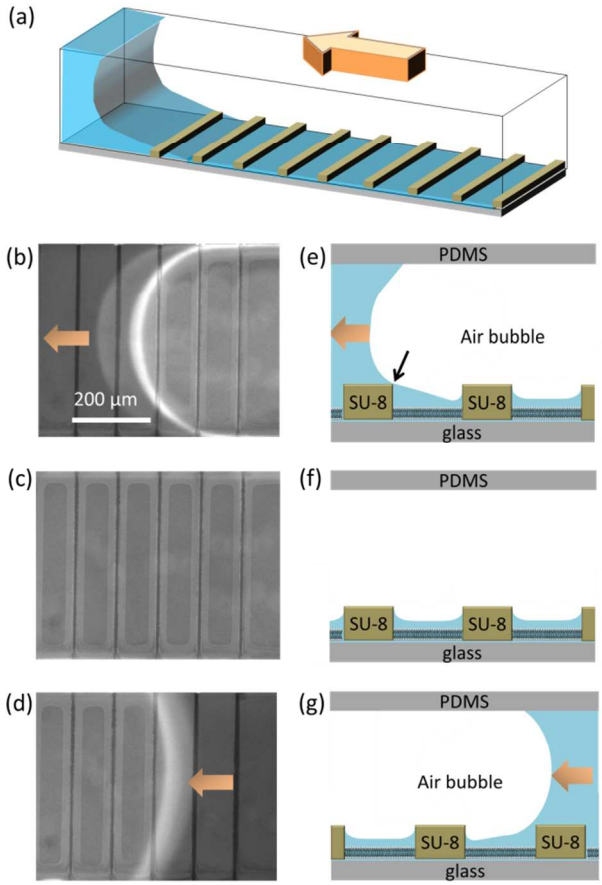

Figure 1. Patterned SU-8 grating structure on the glass surface in a microfluidic device can prevent the air–water interface from directly contacting the confined SLBs. (a) The grating is set perpendicular to the air–water interface moving direction when an air bubble is introduced into the device. (b)(c)(d) Top view fluorescence images taken during air-bubble treatment at 25°C. 0.5 mol% Texas Red DHPE was added into the lipid membrane to reveal the locations of SLBs (bright) and the obstacle grating (dark). The bright curved rings across the channel in (e) and (g) are the air-water interfaces. The slightly brighter regions around the dark grating below an air bubble are probably due to the meniscus light diffraction. (e)(f)(g) Side view Illustrations inside a microchannel at the stages corresponding to (b)(c)(d) respectively

Examining the Integrity of Confined SLBs in the Obstacle Grating with Various Obstacle Distances before Air-Bubble Treatment, under an Air Bubble, and after Rehydration. We formed SLBs (DOPC doped with 0.5 mol% Texas Red DHPE) in the region confined in the obstacle gratings at various distances between the two neighboring obstacles, ranging from 20 μm to 200 μm, as shown in Figure 2(a). After an air bubble was pumped into the channel with the air–water interface moving at a speed of 60 mm/min (3μL/min) (Figure 2(b)), the SLBs confined in the grating at a distance of more than 100 μm were partially destroyed, whereas nearly all of the SLBs confined in the grating at a distance of less than 100 μm remained intact. After the air bubble left the channel and the samples were rehydrated (Figure 2(c)), the SLBs that were intact under an air bubble remained intact. The defects in the destroyed SLBs became unclear but still appeared scratched after rehydration. The low measured diffusivity in the SLBs exhibiting dark defects suggested that those SLBs were partially peeled off or destroyed. As illustrated in Figure 2(d), we hypothesized that the obstacle geometry criteria for the confined SLBs to remain intact are related to the water receding-angle. The left illustration shows that the delamination can easily occur when there is no obstacle. The middle illustration shows that if the distance between the two obstacles to the height of the obstacle (w/h) is much larger than the receding-angle (θ), the water receding tail would still be able to contact and peel off the bilayers. The right illustration shows that only when the ratio is smaller than the angle, the obstacles could truncate the interface before the water receding tail has a chance to contact the bilayers.

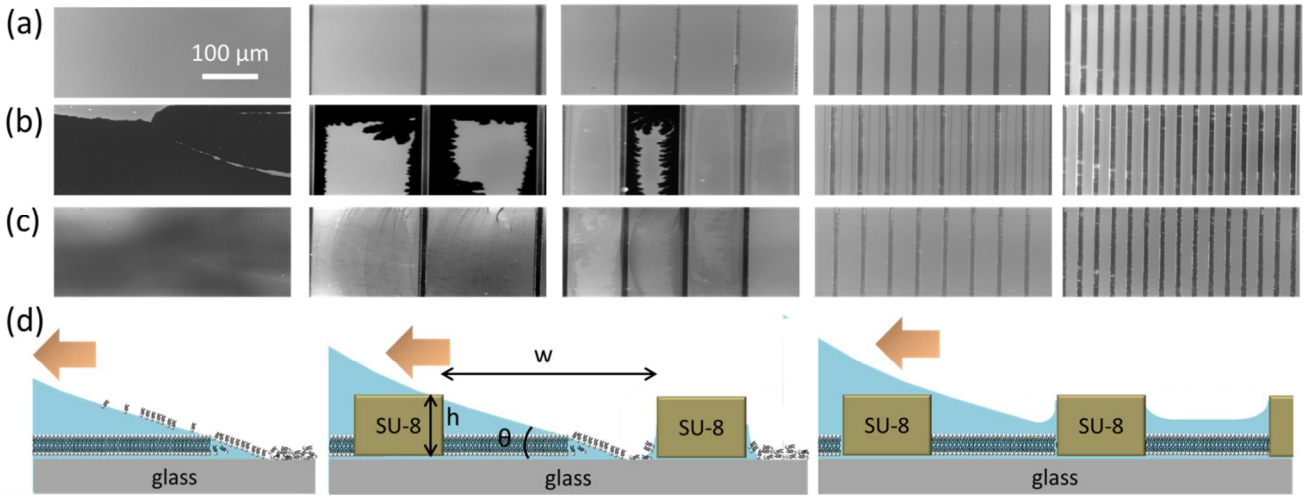

Figure 2 Fluorescence images of the SLBs composed of DOPC with 0.5 mol% Texas Red DHPE: (a) before air-bubble treatment, (b) when an air bubble was in the channel above the samples, and (c) after rehydration. The columns in the rows from the left to right illustrate the conventional unconfined SLBs and those confined in the 200 μm, 100 μm, 40 μm, and 20 μm obstacle gratings. The dark defects generated after air-bubble treatment indicated the peel-off regions of the SLBs. The air–water interfacial speed was 60 mm/min and the system temperature was at 25°C. All of the grating obstacles exhibited a height of 2 μm and a width of 10 μm. (d) Illustrations of how the patterned obstacle geometry could determine whether the air-water interface would have chance to peel off the SLB. From the left to the right: the peel-off situation easily occur in the unconfined SLB; the peel-off situation could occur when the ratio of the distance between the two neighboring obstacles (w) to the obstacle height (h) is much larger than the water-receding contact angle (θ); some water can be retained between the obstacles above the bilayer if the ratio is smaller than θ.

Percentages of the Unaffected Supported Lipid Bilayers Confined in Gratings at Various Obstacle Distances after Air-Bubble Treatment To fulfil the geometry criteria of the obstacle grating structure, we quantified the protection ability of the grating structure at various obstacle distances by performing statistical analyses on the fraction of SLBs confined in the obstacles that remained intact after an air bubble passed by. Table 1 shows the statistical results for the intact fraction of SLBs in the grating structure at obstacle distances (or confinement distances) ranging from 500 μm to 20 μm. The obstacle height was set at 2 μm since fabricating uniform photoresist layer with few-micron thickness is common and easy. In addition, the 2 μm thickness is relatively thin compared to the 100 μm channel height, so that it would not significantly influence the flow pattern or the mass transfer of the species in the bulk solution to the confined SLBs. When the interfacial speed was set at 60 mm/min, the intact fraction decreased as the confinement distance increased. When the distance was less than or equal to 40 μm, all of the lipid bilayers confined in the photoresist gratings were unaffected after an air bubble was introduced, and no visible defects could be observed after rehydration. The SLBs at the confinement distances of 100 μm still showed an unaffected fraction close to 100%. However, when the confinement distance was equal to or greater than 200 μm, the unaffected fraction decreased to less than 20%

Subsequently, we examined whether the movement speed of the air–water interface could influence the obstacle geometry criteria since the movement speed could influence the water-receding angle. The practical reagent flow rate in bioassays is

in the range of a few microliters per minute to hundreds of microliters per minute.[35-37] To evaluate the platform performance under these practical conditions, we applied two flow rates, 60 mm/min and 6000 mm/min, which were at the low end and high end of the practical range, respectively. When the interfacial speed increased 100 fold, we observed that the confinement distance limit decreased from 100 μm to 40 μm. The unaffected fractions of the confinement distances above the limit in the systems with a 6000-mm/min interfacial speed were less than those in the systems with a 60-mm/min interfacial speed. The result showed that the grating geometry criteria were indeed related to the interfacial speed and that our platform with a confinement less than 40 µm protected the SLBs from air bubbles in the typical operating speed range for biosensing applications.

Table 1. Comparison of the unaffected fractions of the SLBs confined in various obstacle distances when the air–water interfacial speeds in the microchannels were 60 mm/min and 6000 mm/min at 25 ˚C. *n* is the number of the experimented confined pieces of SLBs. The obstacle height is 2µm.

Confinement distance (µm)	Unaffected Fraction (60 mm/min)	Unaffected Fraction (6000 mm/min)
500	0.0 % (n=20)	0.0 % (n=18)
400	5.3 % (n=19)	5.3% (n=19)
300	11.1 % (n=18)	5.9 % (n=17)
200	18.5 % (n=27)	18.2 % (n=33)
100	96.2 % (n=26)	57.1% (n=28)
40	100.0 % (n=79)	97.1 % (n=70)
20	100.0 % (n=136)	100.0% (n=96)
10	100.0% (n=260)	100.0% (n=144)
4	100.0 % (n=698)	100.0 % (n=208)

Fluorescence Recovery after Photobleaching for Measuring the Membrane Fluidity before Air-Bubble Treatment, under an Air Bubble, and after Rehydration. Figure 3 shows a comparison of FRAP-measured diffusivities of the intact SLBs (DOPC doped with 0.5 mol% Texas Red DHPE) confined in the obstacle grating structure before and after air-bubble treatment. The diffusivities of the intact SLBs were measured for all of the unaffected SLBs confined in the obstacle gratings after air-bubble treatment. The results showed that the SLBs confined in the obstacle gratings exhibited similar diffusivities before air-bubble treatment and after rehydration, which was 1.66 ± 0.07 $\mu m^2/s$ and 1.61 ± 0.47 $\mu m^2/s$, respectively. The similar diffusivities suggested that the membrane retained its original integrity after air-bubble treatment. By contrast, the diffusivity of the unconfined SLBs decreased substantially after air-bubble treatment. The diffusivity was 1.77 ± 0.07 $\mu m^2/s$ before air-bubble treatment but 0.82 ± 0.63 $\mu m^2/s$ after rehydration, indicating that some defects might have been introduced. The high standard deviation indicated the poor quality of the membrane. In addition, no fluorescence recovery was observed in the unconfined SLBs under an air bubble, but the diffusivity of the confined SLBs remained measurable (1.49 ± 0.06 $\mu m^2/s$) and similar to the diffusivity when they were measured under water. Because water is required for the lateral fluidity of lipid bilayers, this observation suggested water retention above the SLB between the obstacles after an air–water interface passed through. The diffusivities under an air bubble were measured in 5 min after the air bubble was introduced to the platform. We found that if the diffusivities were measured after 30 min, the trapped water would likely evaporate completely, and the diffusivity of the confined SLBs was close to zero. The comparable diffusivity of the confined SLBs before air-bubble treatment, under an air bubble, and after rehydration suggested the promising preservation of lipid bilayers after being exposed to an air–water interface.

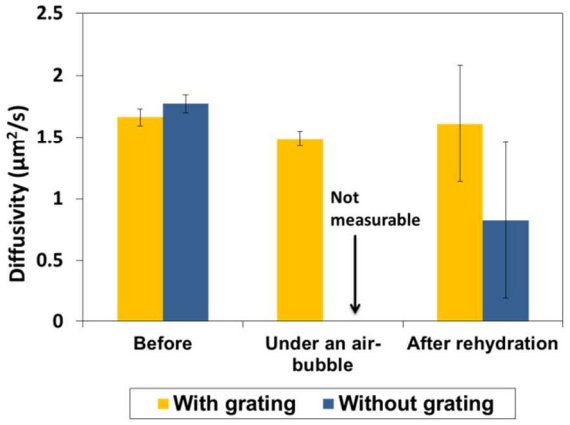

Figure 3. Comparisons of the diffusivities of the confined and unconfined SLBs before air-bubble treatment, under an air bubble, and after rehydration. The SLBs were composed of DOPC doped with 0.5 mol% Texas Red DHPE. The yellow bar represents the diffusivities of SLBs confined in the 100-μm obstacle grating structure exhibiting a height of 2 µm, and the blue bar represents the diffusivities of the unconfined SLBs. No fluorescence recovery was observed in the unconfined SLBs under an air bubble, and thus, the diffusivity was not measurable. The air–water interfacial speed was 60 mm/min and the system temperature was at 25˚C.

Streptavidin-Biotinylated Lipid Interactions Remained in the Developed Platform after Air-Bubble Treatment In this study, we used biotin-streptavidin as a model system to examine whether the receptor–ligand interactions in the confined SLBs remained after air-bubble treatment. We incorporated 0.5 mol% biotinylated lipid in our SLBs as a model receptor and used fluorescence-labeled streptavidin as a model ligand. After the assay procedure was performed and the unbound ligand was removed, as discussed in the Experimental section, the measured fluorescence intensity from the platform was expected to be proportional to

the amount of streptavidin bound to the biotinylated lipid. We used the same batch of fluorescence-labeled streptavidin for all of the experiments and controls to eliminate the fluorescence variation among batches, and the fluorescence dye concentration was less than the quenching limit.

We used the fluorescence intensity for comparing the biotinylated lipid–streptavidin interaction ability of the typical unconfined SLB and confined SLB with or without air-bubble treatment. Figure 3 shows the normalized intensity of the fluorescence labeled streptavidin bond on the SLBs under various conditions. We used the average fluorescence intensity of the bound streptavidin on a typical unconfined unaffected SLB platform as the standard, and all of the other intensities were normalized to it. The left bars represent the SLBs confined in the grating, and the right bars represent the unconfined SLBs with or without air-bubble treatment.

The comparable normalized intensities of bound streptavidin in the confined SLB with and without air-bubble treatment suggested that biotin in the SLB retained its orientation even after an air-bubble passed through the sample. By contrast, the normalized intensity of the unconfined SLB treated with an air bubble was nearly 50% of that without air-bubble treatment. The large standard deviation indicated the poor platform quality. In addition, the fluorescence images of bound streptavidin showed that the unconfined SLB with air-bubble treatment exhibited numerous defects, whereas the confined SLB appeared homogeneous. These results suggested that the bilayer integrity and receptor–ligand interaction ability remained in our platforms after air bubbles passed through.

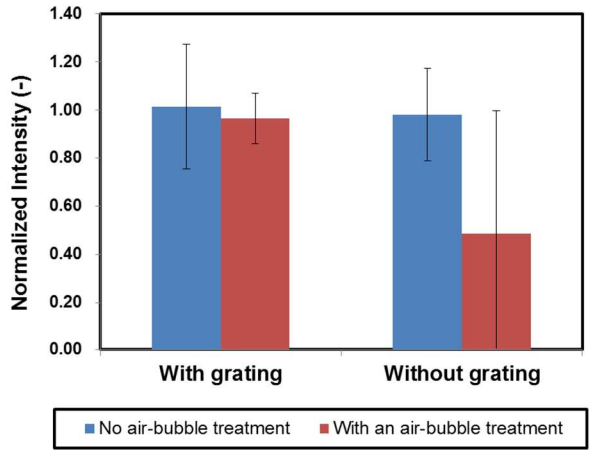

Figure 4. Comparison of the normalized intensity of Alexa Fluor® 488-conjugated streptavidin bound to biotin-X DHPE incorporated in the confined and typical unconfined SLBs. The red bar represents the samples that were treated with air-bubbles before incubation of fluorescence-labeled streptavidin with the SLBs containing biotinylated lipids. The blue bar represents the control samples without air-bubble treatment. The grating width used in this set of experiments was 100 μm, and the air–water interfacial speed was 60 mm/min. The system temperature was at 25˚C. All of the fluorescence intensity data were normalized to the average fluorescence intensity of the typical unconfined SLB samples without air-bubble treatment.

Fluidity and Outside Environment Accessibility Compared with Previously Developed Air-Stable Methods The results of this study showed that addition of grating at a suitable obstacle distance enabled the lipid bilayer platform to retain two crucial properties, membrane fluidity and the outside environment accessibility, after air-bubble treatment. The diffusivities of the confined SLB after air-bubble treatment was 97% of its original diffusivity. In addition, the streptavidin-biotinylated lipid interaction remained mostly unchanged after air-bubble treatment.

To the best of our knowledge, none of the previous air-stable methods have been able to maintain both the high fluidity and high outside environment accessibility of SLB platforms after air-bubble treatment. We mentioned in the Introduction section that previous methods to construct air-stable lipid membranes can be categorized into two groups. One group comprises cross-linked lipids or bound lipids for modifying solid support surfaces to increase the rigidity of lipid membranes; however, the lateral membrane mobility can be substantially reduced. For example, a zirconium-phosphate-modified surface would reduce the diffusivity of a typical SLB on it to 18% of its diffusivity before the modification.[18] The diffusivity of lipid bilayers on a surface with γ-aminopropyl saline modification decreased to approximately 50% of its diffusivity before the modification.[21] Positively charged lipid bilayers had a strong electrostatic interaction with a negatively charged PDMS surface; however, the interaction also affected the diffusivity and reduced the diffusivity to 49% of the SLB diffusivity on a typical glass surface.[22] The second group involves using biomolecules, such as trehalose,[24-29] α-α-galacto-trehalose,[24] and streptavidin,[23] to cover the surface of SLBs for protecting lipid bilayers from delamination. Although most of the methods in the second category retain high diffusivities, the biomolecules covering the SLBs can block the interactions of the ligand in the bulk solutions and receptors in the SLBs. All of these comparisons suggested that the proposed method can effectively preserve the two crucial properties of SLB platforms for biosensing applications and is markedly improved compared with previously developed air-stable methods.

Conclusions

In this study, we used a patterned obstacle grating structure for protecting supported lipid bilayers (SLBs) in a microfluidic device from being destroyed by air bubbles during reagent exchange and transport. The possible protection mechanism is that the grating obstacles can trap some water above the lipid bilayers to prevent the air–water interface from directly contacting and peeling the lipid bilayers. The gratings were patterned perpendicular to the reagent flow direction in a microchannel to achieve optimal water-retention ability between the grating obstacles. We observed that the grating structure geometry criterion was associated with the air–water interface movement speed. The required confinement distance was shorter when the interfacial speed was faster, likely because the speed is related to the water-receding angle. We showed that, at a confinement-distance less than 40μm, our platform with grating height equal to 2μm can provide

promising protection to SLBs from air bubbles at the typical biosensing operating speed range (60 mm/min to 6000 mm/min). The FRAP measurement for the unaffected confined SLBs showed that the fluidity remained nearly the same as the original fluidity after air-bubble treatment. In addition, streptavidin-biotinylated lipid interactions measured from the fluorescence intensity showed that the receptor–ligand interaction ability remained similar after air-bubble treatment. Compared with other previously air-stable methods, the method developed here more effectively retains membrane fluidity and the accessibility of its component to the outside environment. The physically confined SLB platform integrated with a microfluidic device for reagent transport and exchange has great potential to be applied with surface analytical tools to create highly robust in vitro cell-membrane-related bioassays in the future.

Acknowledgements

We thank National Taiwan university and National Science Council in Taiwan for the funding support for this work (NSC102-2221-E-002-153-MY3).

References

1. M. Bally, K. Bailey, K. Sugihara, D. Grieshaber, J. Voros and B. Stadler, *Small*, 2010, **6**, 2481-2497.
2. E. Sackmann, *Science*, 1996, **271**, 43-48.
3. M. Rough, *MRS bulletin*, 2006, **31**, 537.
4. J. T. Groves and M. L. Dustin, *Journal of immunological methods*, 2003, **278**, 19-32.
5. J. T. Groves and S. G. Boxer, *Accounts of chemical research*, 2002, **35**, 149-157.
6. C. Bieri, O. P. Ernst, S. Heyse, K. P. Hofmann and H. Vogel, *Nature biotechnology*, 1999, **17**, 1105-1108.
7. V. Yamazaki, O. Sirenko, R. J. Schafer, L. Nguyen, T. Gutsmann, L. Brade and J. T. Groves, *BMC biotechnology*, 2005, **5**, 18.
8. K. S. Phillips and Q. Cheng, *Analytical chemistry*, 2005, **77**, 327-334.
9. Y. Dong, K. S. Phillips and Q. Cheng, *Lab on a chip*, 2006, **6**, 675-681.
10. P. S. Cremer and S. G. Boxer, *The Journal of Physical Chemistry B*, 1999, **103**, 2554-2559.
11. J. T. Groves, N. Ulman, P. S. Cremer and S. G. Boxer, *Langmuir*, 1998, **14**, 3347-3350.
12. E. E. Ross, B. Bondurant, T. Spratt, J. C. Conboy, D. F. O'Brien and S. S. Saavedra, *Langmuir*, 2001, **17**, 2305-2307.
13. M. Halter, Y. Nogata, O. Dannenberger, T. Sasaki and V. Vogel, *Langmuir*, 2004, **20**, 2416-2423.
14. J. C. Conboy, S. Liu, D. F. O'Brie and S. S. Saavedra, *Biomacromolecules*, 2003, **4**, 841-849.
15. F. Albertorio, A. J. Diaz, T. Yang, V. A. Chapa, S. Kataoka, E. T. Castellana and P. S. Cremer, *Langmuir*, 2005, **21**, 7476-7482.
16. Y. Deng, Y. Wang, B. Holtz, J. Li, N. Traaseth, G. Veglia, B. J. Stottrup, R. Elde, D. Pei, A. Guo and X. Y. Zhu, *Journal of the American Chemical Society*, 2008, **130**, 6267-6271.
17. B. P. Oberts and G. J. Blanchard, *Langmuir*, 2009, **25**, 2962-2970.
18. R. M. Fabre and D. R. Talham, *Langmuir*, 2009, **25**, 12644-12652.
19. Y. Fang, *Chemical Physics Letters*, 2011, **512**, 258-262.
20. Y. Fang, *Journal of the American Chemical Society*, 2006, **128**, 3158-3159.
21. Y. Fang, A. G. Frutos and J. Lahiri, *Journal of the American Chemical Society*, 2002, **124**, 2394-2395.
22. K. S. Phillips, Y. Dong, D. Carter and Q. Cheng, *Analytical Chemistry*, 2005, **77**, 2960-2965.
23. M. A. Holden, S.-Y. Jung, T. Yang, E. T. Castellana and P. S. Cremer, *Journal of the American Chemical Society*, 2004, **126**, 6512-6513.
24. F. Albertorio, V. A. Chapa, X. Chen, A. J. Diaz and P. S. Cremer, *Journal of the American Chemical Society*, 2007, **129**, 10567-10574.
25. C. W. Harland, Z. Botyanszki, D. Rabuka, C. R. Bertozzi and R. Parthasarathy, *Langmuir*, 2009, **25**, 5193-5198.
26. S. V. Bennun, R. Faller and M. L. Longo, *Langmuir : the ACS journal of surfaces and colloids*, 2008, **24**, 10371-10381.
27. J. V. Ricker, N. M. Tsvetkova, W. F. Wolkers, C. Leidy, F. Tablin, M. Longo and J. H. Crowe, *Biophysical Journal*, 2003, **84**, 3045-3051.
28. S. Chiantia, N. Kahya and P. Schwille, *Langmuir*, 2005, **21**, 6317-6323.
29. A. E. Oliver, E. L. Kendall, M. C. Howland, B. Sanii, A. P. Shreve and A. N. Parikh, *Lab on a chip*, 2008, **8**, 892-897.
30. J. Bico, U. Thiele and D. Quéré, *Colloids and Surfaces A: Physicochemical and Engineering Aspects*, 2002, **206**, 41-46.
31. R. J. Jackman, D. C. Duffy, E. Ostuni, N. D. Willmore and G. M. Whitesides, *Analytical Chemistry*, 1998, **70**, 2280-2287.
32. F. Walther, P. Davydovskaya, S. Zürcher, M. Kaiser, H. Herberg, A. M. Gigler and R. W. Stark, *Journal of Micromechanics and Microengineering*, 2007, **17**, 524.
33. J. Zhang, W. Zhou, M. B. Chan-Park and S. R. Conner, *Journal of the Electrochemical Society*, 2005, **152**, C716-C721.
34. C.-T. Han and L. Chao, *ACS Applied Materials & Interfaces*, 2014, **6**, 6378-6383.
35. L. G. Fägerstam, Å. Frostell-Karlsson, R. Karlsson, B. Persson and I. Rönnberg, *Journal of Chromatography A*, 1992, **597**, 397-410.
36. K. E. Komolov, I. I. Senin, P. P. Philippov and K.-W. Koch, *Analytical chemistry*, 2006, **78**, 1228-1234.
37. J. Lahiri, L. Isaacs, J. Tien and G. M. Whitesides, *Analytical Chemistry*, 1999, **71**, 777-790.